Chapter 4

Microstructure and Properties of Casting Magnesium Alloys Designed to Work in Elevated Temperature

Andrzej Kiełbus

Additional information is available at the end of the chapter

http://dx.doi.org/10.5772/intechopen.80291

Abstract

Magnesium alloys are widely used in aerospace and automotive industry due to their low density, good mechanical properties, and good castability. Their main disadvantage is low maximum working temperature (about 120°C for Mg-Al alloys). This led to the development of Mg-Al-RE or Mg-RE-Zr alloys, which can work up to 250°C. The chapter will relate to the sand cast and high pressure die cast magnesium alloys. Material for the research consisted of six magnesium casting alloys: AE44, AJ62, WE54, EV31A, and for comparison AZ91 and AM50. The influence of casting and heat treatment parameters on the microstructure and mechanical properties will be introduced. The relationship between the initial structure, casting parameters, phase composition, and mechanical properties in magnesium alloys will be presented.

Keywords: magnesium alloys, sand casting, high-pressure die casting, heat treatment, microstructure, phase composition, mechanical properties

1. Introduction

Due to chemical composition, casting magnesium alloys are divided into two groups [1]. The first group includes alloys containing from 3 to 10% Al with the addition of Zn and Mn. They are characterized by a low cost of manufacture, good tensile strength, elongation, and resistance to atmospheric corrosion. The most popular representative of this group of alloys is AM50 alloy mainly for die casting and AZ91 that can be cast by sand and die casting method. The main advantage of these alloys is their relatively low price, while their disadvantage is low operating temperature—below 120°C [2]. To increase the operating temperature of Mg-Al alloys, alloying elements are introduced, such as rare earth metals, strontium, calcium, and

other. Application of rare earth elements to Mg-Al alloys causes a formation of stable thermodynamic phases at the grain boundaries, which provides motivation for improving creep resistance [3]. In particular, the microstructure is connected by the $Al_{11}RE_3$ phase, which is characterized by a high thermodynamic stability to the temperature of ~180°C. The high thermodynamic stability of this phase uses all the aluminum atoms to form this phase during spheroidization, which prevents the $Mg_{17}Al_{12}$ phase from forming. Consequently, these alloys may be applied in the automotive industry for engine elements, gearing, oil pans, and other structural materials working at temperatures of ~180°C [4, 5]. High prices of rare earth elements and their small availability oblige us to search for alternative solutions [6]. Some of those solutions are Mg-Al alloys to which strontium is added. The α-Mg solid solution and eutectic, which consists of one or more intermetallic phases, form the microstructure of Mg-Al-Sr alloys. The Al_4Sr phase is mainly observed in alloys with no more than 5% Al; however, the undesirable $Mg_{17}Al_{12}$ phase can be found in alloys with no more than 6% concentration of Al [7, 8].

The second group includes alloys containing mainly Zn, RE, and Y, without the addition of Al, but always with the addition of Zr. These alloys can be used at a temperature higher than 120°C (up to 250°C), but the price of alloy additions increases the cost of their production. They are mainly used as sand castings. In this group, the most widely used alloys are WE54 and the latest EV31A (Elektron 21) [1]. WE54 magnesium alloy reaches high specific strength, creep resistance, and corrosion resistance up to a temperature of 250°C. The strength of this alloy is achieved essentially via precipitation strengthening. Depending on the aging temperature and time, the precipitating sequence in WE alloys has been reported to involve the formation of phases designated β″, β′, and β [9, 10]. EV31A is magnesium-based sand casting alloy containing neodymium, gadolinium, and zinc for used to approximately 200°C. This alloy has high strength, good corrosion resistance, and excellent castability. In as-cast condition, EV31A alloy is characterized by a solid solution structure α-Mg with eutectic α-Mg + Mg_3(Nd, Gd) intermetallic phase on grain boundaries. Depending on the aging temperature and time, the decomposition of α-Mg supersaturated solid solution is as follows: α-Mg → β″ → β′ → β(Mg_3RE) → $Mg_{41}Nd_5$ [11]. EV31A is being used in both civil and military aircraft and also in the automobile (motorsport) industry [12].

2. Material for research

The material used for the research consisted of the AM50, AZ91, AE44, AJ62, EV31A, and WE54 casting magnesium alloys. The chemical composition of these alloys is provided in **Table 1**.

Alloy	Al	Mn	Zn	Si	Ce	La	Sr	Nd	Gd	Y	Zr	Mg
AM50	4.9	0.45	—		—	—	—	—	—	—	—	Balance
AZ91	8.9	0.24	0.6	0.1	—	—	—	—	—	—	—	
AE44	4.25	0.18	—		2.35	1.07	—	0.59	—	—	—	
AJ62	6.15	0.42	—		—	—	2.1	—	—	—	—	
WE54	—	—	—		—	—	—	1.7	—	5.0	0.55	
EV31A	—	0.001	0.4				—	2.7	1.2	—	0.49	

Table 1. The chemical composition of the investigated magnesium alloys in wt.%.

http://dx.doi.org/10.5772/intechopen.80291

3. Research methodology

The chemical composition of investigated alloys was measured on the SPEKTROMAX spectrometer. Sand casting was carried out at 700°C (AM50, AZ91, AE44, and AJ62) and 780°C (WE54 and EV31A) temperature. Hot chamber die casting was performed at 650°C (AM50 and AJ62) and 680°C (AE44) temperature. Long-term annealing of AM50 and AZ91 alloys was conducted at two different temperatures: 180 and 250°C for 500–5000 h with air cooling. For AE44 and AJ62 alloys, annealing at temperature 350°C was additionally applied. The as-cast specimens of WE54 and EV31A alloys were solution treated at 520°C for 8 h and quenched into water. Aging treatments were performed at 200, 250, 350, and 420°C for 4–1000 h with air cooling.

For the microstructure observation, an OLYMPUS GX71 metallographic microscope and HITACHI S-3400 N scanning electron microscope were used. TEM examination was carried out on a Tecnai G^2 transmission electron microscope equipped with a high-angle annular dark-field detector (HAADF) and energy-dispersive X-ray (EDX) spectrometer. Metallographic specimens were made in accordance with the methodology developed at the Institute of Materials Engineering at the Silesian University of Technology. X-ray diffraction patterns were collected using an X-Pert Philips diffractometer. Hardness tests have been performed with a Vickers indenter. The examination of the mechanical properties was conducted on an MTS-810 machine at ambient (ca. 20°C) and 200°C.

4. Microstructure and properties of Mg-Al alloys

4.1. AM50 and AZ91 alloys

Sand casting AM50 alloy is characterized by the structure of α-Mg solid solution with precipitates of two types of $Mg_{17}Al_{12}$ phases (**Figure 1a**). First one of massive morphology, together with the solid solution, forms partially divorced eutectic (continuous $Mg_{17}Al_{12}$ + α-Mg) at the grain boundaries. Divorced eutectic $Mg_{17}Al_{12}$ + α-Mg is characterized by the presence of "islands" of α-Mg solid solution, solidifying due to eutectic reaction, which are surrounded by $Mg_{17}Al_{12}$ phase precipitates. The second one of plate morphology is created as a result of discontinuous diffusional transformation. Discontinuous precipitation occurs mostly in the α-Mg regions near the massive $Mg_{17}Al_{12}$ phase on the solid solution α-Mg grain boundaries in regions with higher aluminum. The volume fraction of α-Mg solid solution within $Mg_{17}Al_{12}$ phase precipitates is much smaller than it appears from the balance system. Moreover, globular precipitates of Al_8Mn_5 phase occur in the AM50 alloy.

Casting magnesium alloy AZ91 is the most popular and relatively cheap in comparison with other magnesium alloys available on the market. Aluminum causes an increase in tensile strength and hardness of the alloy but only to a temperature of 120°C. The AZ91 magnesium alloy, like AM50 alloy in as-cast condition, was characterized by a solid solution α-Mg with discontinuous and continuous precipitates of the $Mg_{17}Al_{12}$ phase (**Figure 1b**), with the difference that the volume fraction of the $Mg_{17}Al_{12}$ phase is higher in the AZ91 alloy. Moreover, the occurrence of Mg_2Si and Al_8Mn_5 phases has been provided.

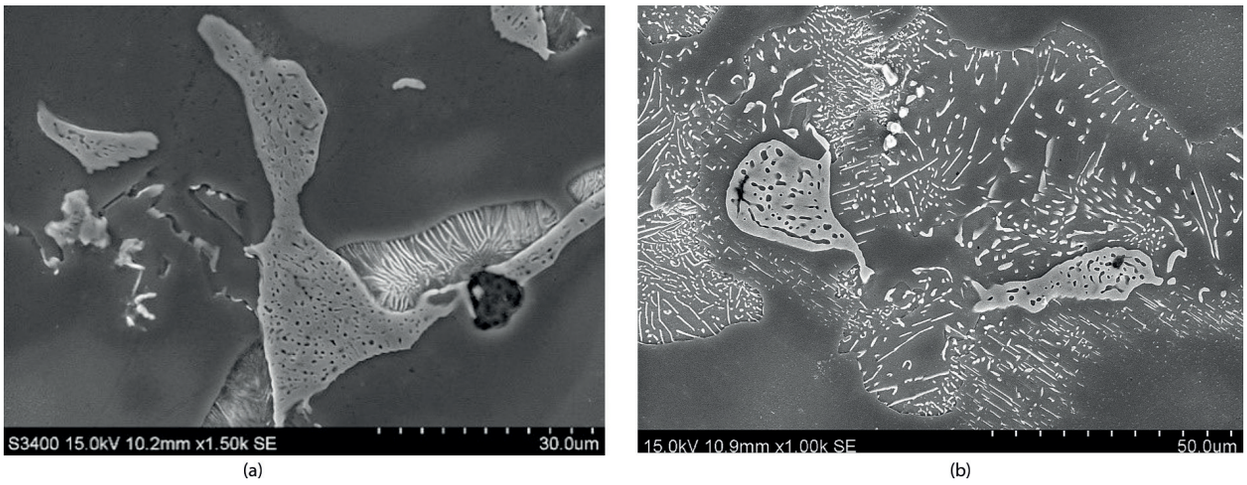

Figure 1. The microstructure of Mg-Al alloys after sand casting, AM50 (a), AZ91 (b), SEM.

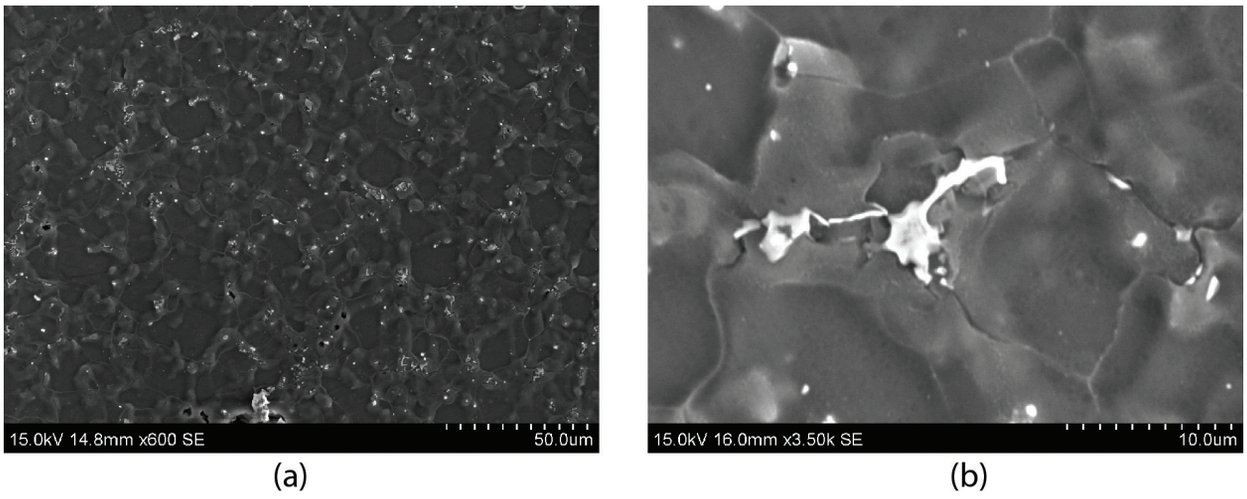

Figure 2. The microstructure of AM50 alloy after die-casting, SEM.

After die casting, the structure of AM50 alloy is characterized by significant grain refining of the α-Mg solid solution; however, $Mg_{17}Al_{12}$ phase, together with the α-Mg solid solution, forms fully divorced eutectic on the grain boundaries of α-Mg solid solution (**Figure 2**).

During annealing, precipitation of $Mg_{17}Al_{12}$ phase proceeds continuously and discontinuously. In sand casting, firstly, as a result of discontinuous precipitation, precipitates of plate $Mg_{17}Al_{12}$ phase are formed. The process is started on the grain boundaries of the α-Mg solid solution and consists of cellular growth of plate precipitation of $Mg_{17}Al_{12}$ phase in the direction of the central part of the solid solution grain. The growth of lamellar precipitates runs continuously until the alloy matrix reaches the equilibrium composition. The volume fraction of lamellar areas and the distance between the lamellas increases with the rise of temperature, aging time, and an aluminum content in the supersaturated areas. The second step is the coagulation of plate precipitates and the beginnings of continuous precipitation of $Mg_{17}Al_{12}$ phase in zones of increasing content of aluminum. Further annealing causes growth and coagulation of both types of precipitates (**Figure 3**). The extension of annealing time to 5000 h or increasing temperature of annealing to the 250°C causes continuous growing and coagulation of precipitation of $Mg_{17}Al_{12}$ phase (**Figure 4**).

http://dx.doi.org/10.5772/intechopen.80291

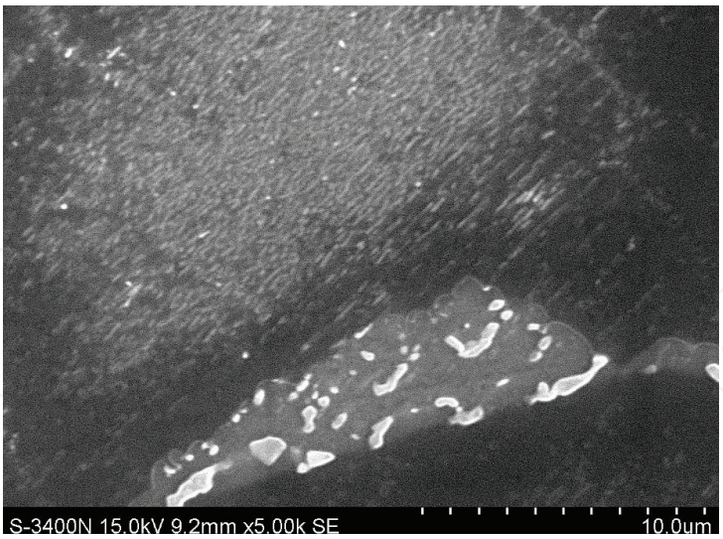

Figure 3. The zones of continuous and coalesced precipitates of $Mg_{17}Al_{12}$ phase in AM50 alloy, after annealing at 180°C/500 h/air.

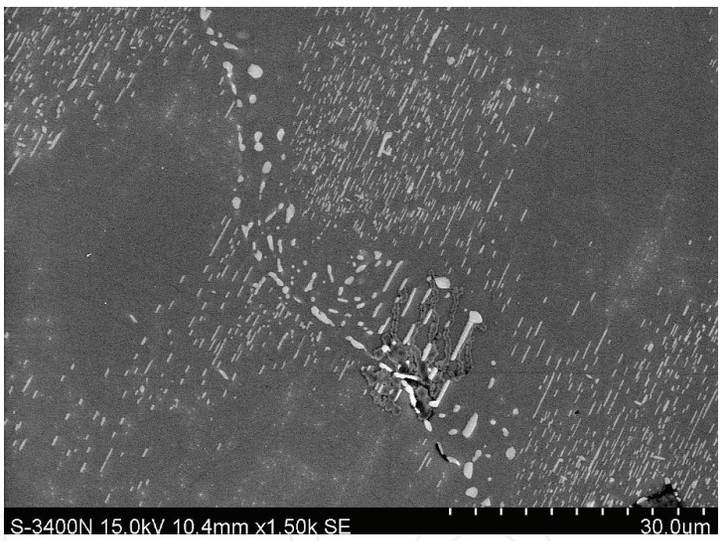

Figure 4. The microstructure of sand casting AM50 alloy, after annealing at 250°C/5000 h/air.

The precipitation processes during long-term annealing in die casting AM50 magnesium alloy proceed similarly as in sand casting, but the difference is that discontinuous precipitation of $Mg_{17}Al_{12}$ phase is not observed in the first step of the process. After 4000 h of annealing, a big, coagulated precipitation of $Mg_{17}Al_{12}$ phase makes the structure of the alloy on the grain boundaries of α-Mg solid solution (**Figure 5**). Long-term annealing at 250°C temperature causes growth and coagulation of continuous precipitates of $Mg_{17}Al_{12}$ phase (**Figure 6**).

The precipitation processes of the $Mg_{17}Al_{12}$ phase during long-term annealing of sand casts resulted in the growth of the hardness of the alloy alongside with lengthening the annealing time. However, in die casts, the structure of the alloy undergoes degradation in the result of precipitation and the coagulation of $Mg_{17}Al_{12}$ phase, what reduces hardness significantly (**Figure 7**).

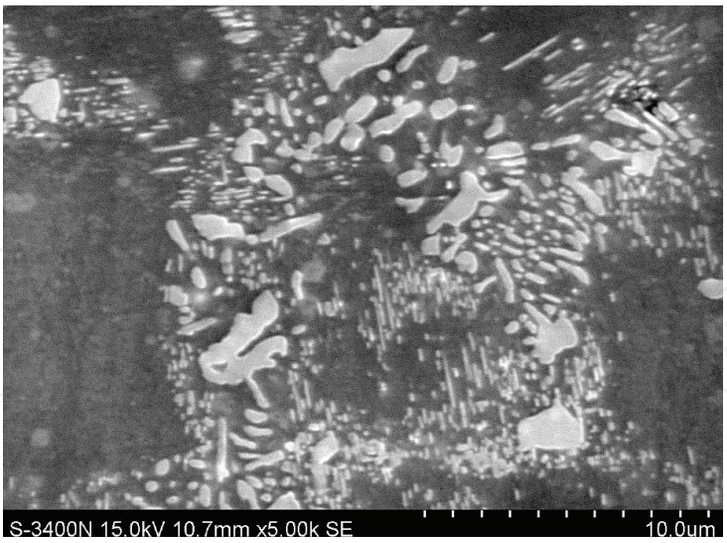

Figure 5. Coalesced continuous precipitates of $Mg_{17}Al_{12}$ phase in die-casting AM50 alloy after annealing at 180°C/4000 h/air.

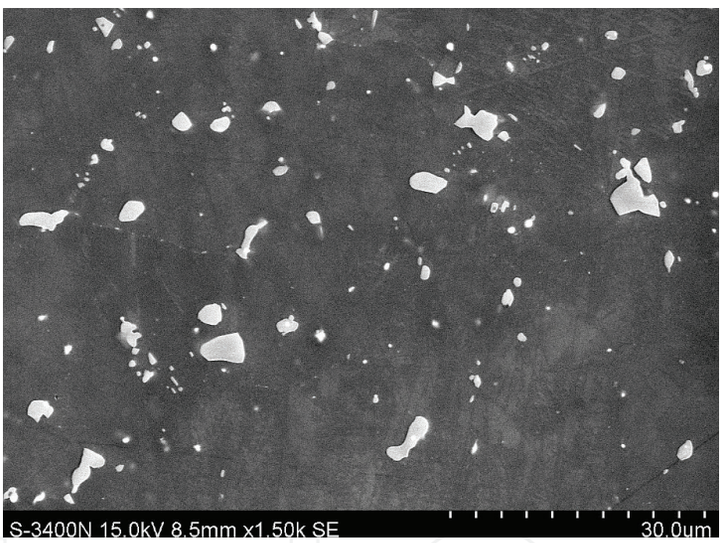

Figure 6. Coagulation of continuous precipitates of $Mg_{17}Al_{12}$ phase in die-casting AM50 alloy after annealing at 250°C/4000 h/air.

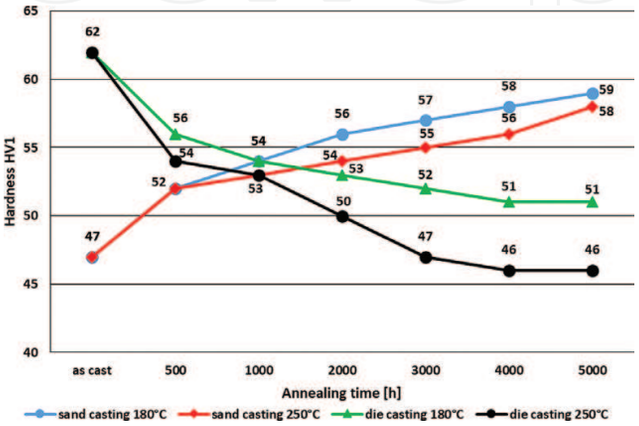

Figure 7. Influence of temperature and annealing time on the hardness of the AM50 alloy.

http://dx.doi.org/10.5772/intechopen.80291

AM50 and AZ91 alloys due to very good mechanical properties at an ambient temperature and low at elevated temperature can only be used at up to 120°C. This is connected with the presence of $Mg_{17}Al_{12}$ phase, which helps to increase the tensile strength at an ambient temperature but decreases the mechanical properties at an elevated temperature.

5. Microstructure and properties of Mg-Al-X (RE, Sr) alloys

5.1. AE44 alloy

Addition of rare earth elements (mainly cerium, lanthanum, and neodymium) to an alloy with 4% aluminum increases durability and operating temperature of the alloy. The microstructure of the AE44 alloy after sand casting is dominated by the $Al_{11}RE_3$ phase. Moreover, the Al_2RE and $Al_{10}RE_2Mn_7$ phases occur (**Figure 8a**). Die-casting causes grain refining of the solid solution. Diverse morphology of the interdendritic phases occurs at the α-Mg grain boundaries. Needle precipitates of the $Al_{11}RE_3$ phase together with the α-Mg solid solution form a eutectic like–fiber morphology. In contrast to the situation for sand casting, the metastable $Al_{2.12}RE_{0.88}$ phase forms next to eutectic areas (**Figure 8b**).

The $Al_{11}RE_3$ and Al_2RE compounds are typical in Mg-Al-RE alloys. The $Al_{2.12}RE_{0.88}$ is not an equilibrium phase in the binary Al-RE (Al-La) system. The presence of this compound is a result of rapid crystallization during die casting and that it is a metastable phase at room temperature. The $Al_{2.12}RE_{0.88}$ compound was not found in slowly cooled sand cast AE44 alloy.

After long-term annealing at 180°C for 3000 h, the structure of AE44 alloy reveals no significant changes. Continuous precipitation of the $Mg_{17}Al_{12}$ phase is observed only in aluminum supersaturated areas of the α-Mg solid solution in the sand cast alloy (**Figure 9**). The morphology of $Mg_{17}Al_{12}$ phase suggests continuous precipitation from a supersaturated solid solution. These precipitates were occasionally observed in the alloy. Increasing the annealing temperature to 250°C accelerates the process of fragmentation and spheroidization of $Al_{11}RE_3$ phase precipitates (**Figure 10**).

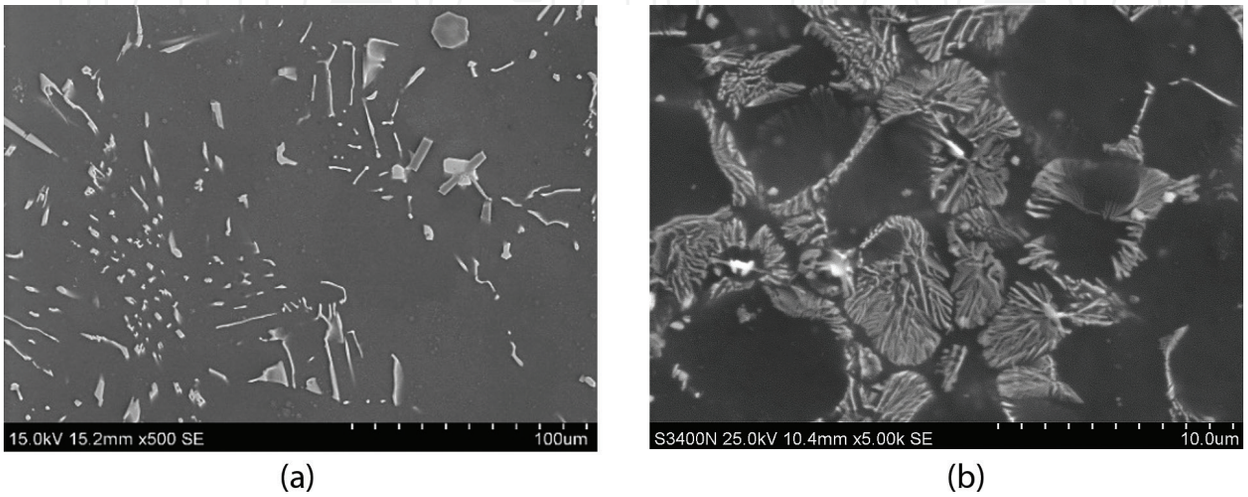

Figure 8. The microstructure of the AE44 alloy after sand casting (a), die casting (b), SEM.

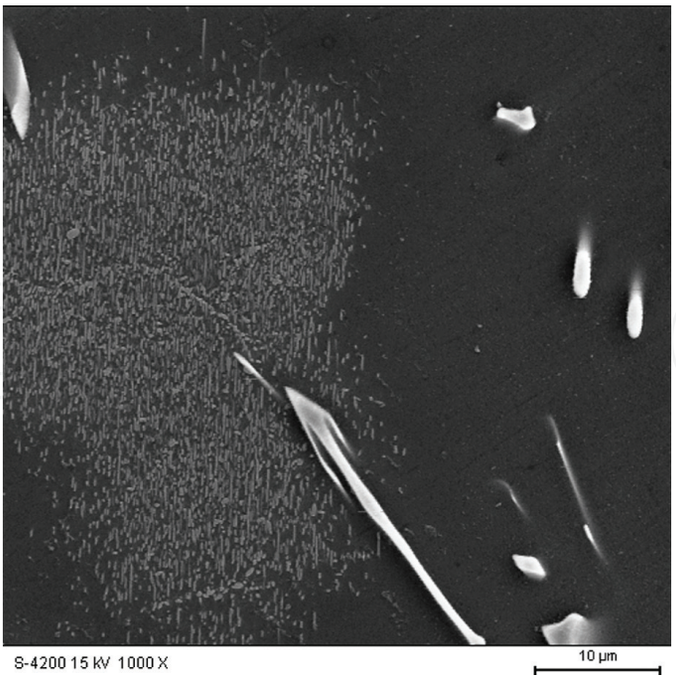

Figure 9. Precipitates of $Mg_{17}Al_{12}$ phase in the sand cast AE44 alloy after annealing at 180°C/3000 h.

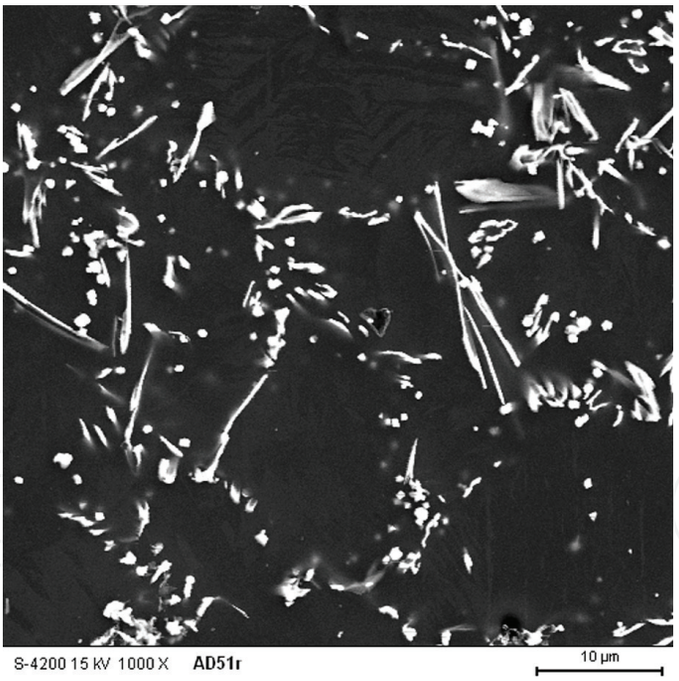

Figure 10. Fragmentation of $Al_{11}RE_3$ phase precipitates in the die-cast AE44 alloy after annealing at 250°C/3000 h.

During long-term annealing of die-cast AE44 alloy, the metastable $Al_{2.12}RE_{0.88}$ phase undergoes a transition into the equilibrium Al_2RE phase (**Figure 11**).

An increase in the hardness (only sand cast) after annealing at the temperature of 180°C is caused by the separation of $Mg_{17}Al_{12}$ phase in the areas of increased aluminum content (**Figure 12a**). The fragmentation and spheroidization of $Al_{11}RE_3$ phase after annealing at

http://dx.doi.org/10.5772/intechopen.80291

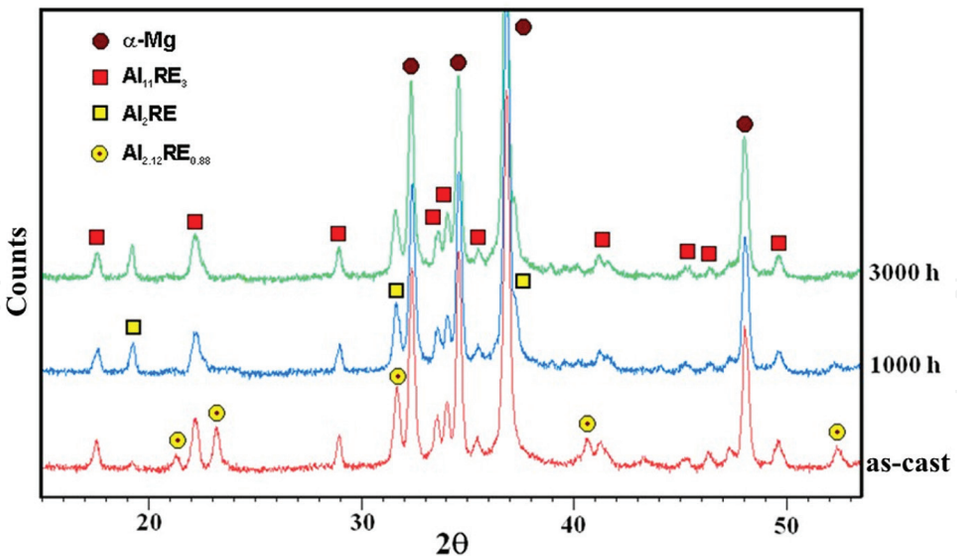

Figure 11. X-ray diffractions of the die-casting AE44 alloy after annealing for 1000 and 3000 h at the temperature of 180°C.

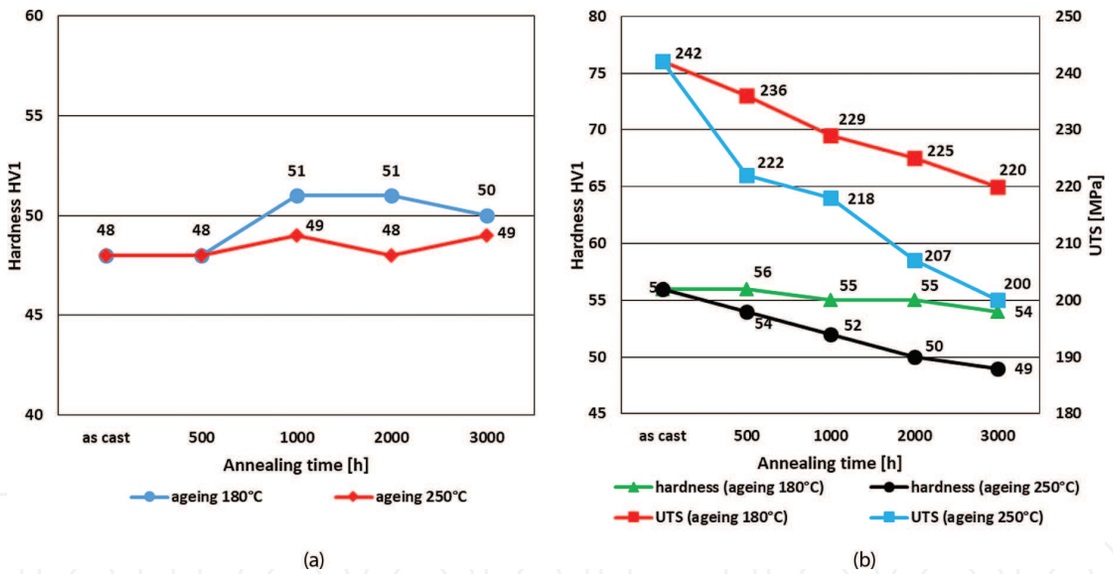

Figure 12. The influence of temperature and annealing time on the hardness and tensile strength of the AE44 alloy after sand casting (a) and die casting (b).

temperatures of 180 and 250°C caused a significant decrease in hardness and tensile strength of die casting AE44 (**Figure 12b**).

5.2. AJ62 alloy

The AJ62 alloy is characterized by the structure of the α-Mg solid solution with precipitates of intermetallic phases of type: $(Al, Mg)_4Sr$, $Al_3Mg_{13}Sr$, and Mn_5Al_8. The $(Al, Mg)_4Sr$ phase and the solid solution form eutectic of α-Mg + $(Al, Mg)_4Sr$. However, the $Al_3Mg_{13}Sr$ phase occurs at the grain boundaries of the α-Mg solid solution in the direct surroundings of eutectic areas. Globular precipitates of the Mn_5Al_8 phase occur at grain boundaries and inside the grains of

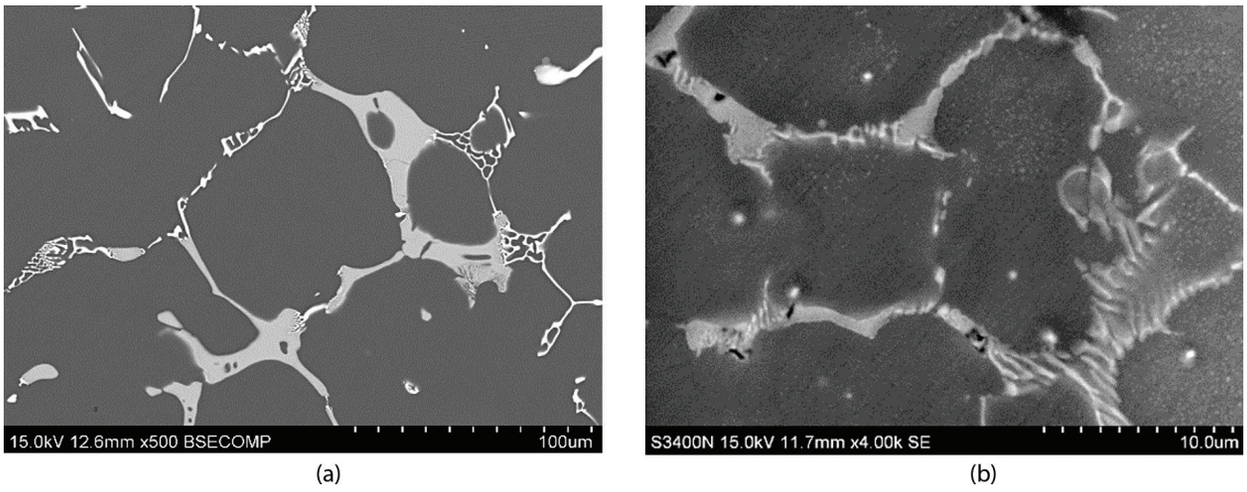

Figure 13. The microstructure of AJ62 alloy after sand casting (a), die casting (b), SEM.

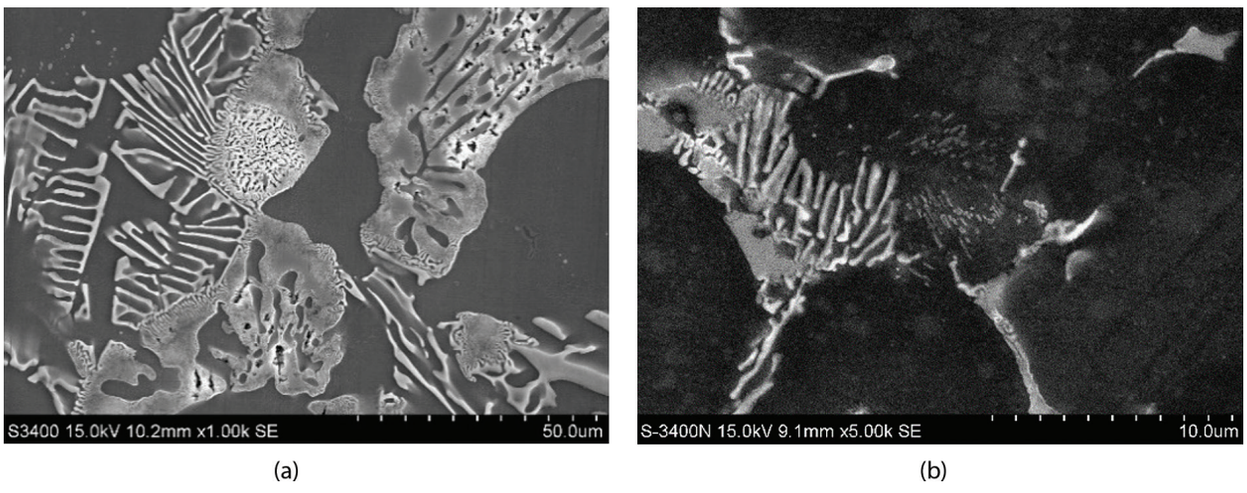

Figure 14. Precipitates of $Mg_{17}Al_{12}$ and initial decomposition of $Al_3Mg_{13}Sr$ phase after annealing of sand casting for 500 h at 250°C (a) and die casting for 4000 h at 180°C (b).

the α-Mg solid solution. In the thin-wall die casts, eutectic α-Mg + $(Al, Mg)_4Sr$ occurs at the grain boundaries. Moreover, for thick-wall casting, which is characterized by a lower cooling rate, the $Al_3Mg_{13}Sr$ phase occurs (**Figure 13**).

The applied casting technology has no influence on the type of changes in the AJ62 alloy microstructure during long-term annealing. The first step occurs at ~180°C (250°C/500 h) and is characterized by precipitation of the $Mg_{17}Al_{12}$ phase in areas of higher aluminum volume (as in AE44 alloy) and the beginning of $Al_3Mg_{13}Sr$ phase decomposition (**Figure 14**).

Decomposition of this phase results in the formation of plate precipitates of the $(Al, Mg)_4Sr$ phase separated by areas of α-Mg solid solution. The second step occurs at ~250°C and consists of complete degradation of the $Al_3Mg_{13}Sr$ phase by the reaction $Al_3Mg_{13}Sr \rightarrow (Al, Mg)_4Sr$ + α-Mg (**Figure 15**). The third step occurs above 300°C. In the α-Mg solid solution,

http://dx.doi.org/10.5772/intechopen.80291

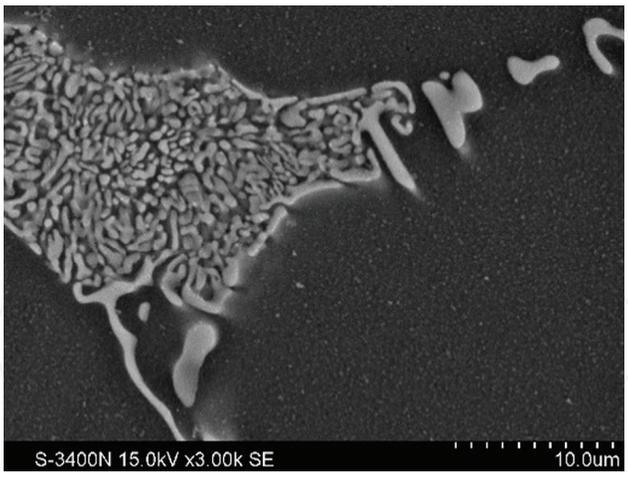

Figure 15. Complete decomposition of $Al_3Mg_{13}Sr$ phase in sand-cast AJ62 alloy after annealing for 1000 h at 350°C, SEM.

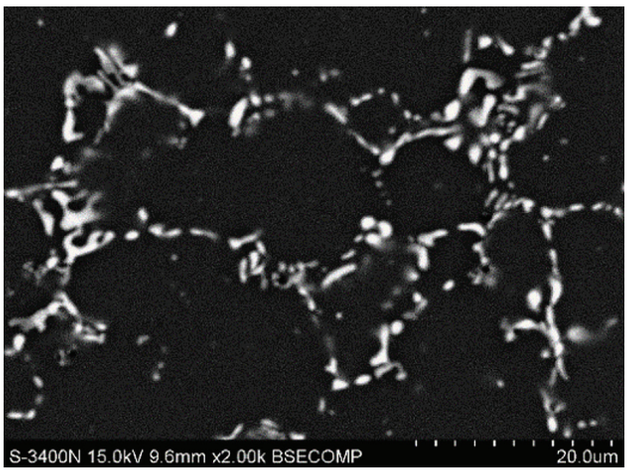

Figure 16. Coagulation of $(Al, Mg)_4Sr$ phase precipitates in die-cast AJ62 alloy after annealing for 4000 h at 350°C, SEM.

there are only precipitates of the primary and secondary (generated from $Al_3Mg_{13}Sr$ phase decomposition) $(Al, Mg)_4Sr$ phase. Long-term annealing at this temperature leads to fragmentation and coagulation of $(Al, Mg)_4Sr$ phase precipitates (**Figure 16**).

The hardness and tensile strength evolution of AJ62 alloy as a function of aging time for isothermal aging at 200, 250, and 350°C is shown in **Figure 17**.

Increase in hardness after annealing at the temperature of 180°C as well as in the first stage of annealing at the temperature of 250°C (only sand cast) is caused by the separation of $Mg_{17}Al_{12}$ phase in the areas of increased aluminum content. The hardness of the die cast, unlike of sand cast, does not decrease after annealing at the temperature of 250°C. It is related to the lower number of $Al_3Mg_{13}Sr$ phase precipitates. The decomposition of $Al_3Mg_{13}Sr$ phase and coagulation of $(Al, Mg)_4Sr$ phase precipitates after annealing at the temperature of 350°C cause a significant decrease in hardness and tensile strength of AJ62 alloy, regardless of applied casting technology.

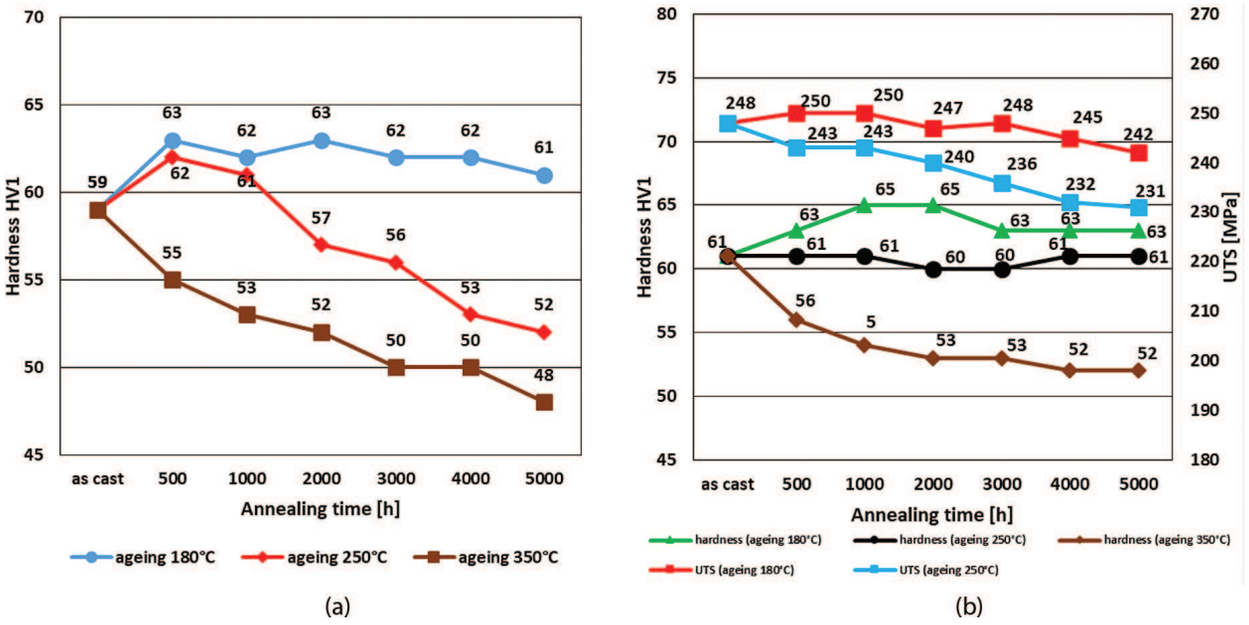

Figure 17. The influence of temperature and annealing time on the hardness and tensile strength of the AJ62 alloy after sand casting (a) and die casting (b).

6. Microstructure and properties of Mg-Zr-X alloys

6.1. WE54 alloy

The WE54 alloy in as-cast condition was characterized by a solid solution structure α-Mg with eutectic α-Mg + β on grain boundaries (**Figure 18**). Equilibrium β phase is isomorphic to the Mg_5Gd phase and is identified as a $Mg_{14}Nd_2Y$ phase. Moreover, the occurrence of MgY, Mg_2Y, and $Mg_{24}Y_5$ phases has been provided [13]. Also, the zirconium-rich core areas have been observed. Zirconium-rich core areas are ellipsoidal or nearly circular (**Figure 19**).

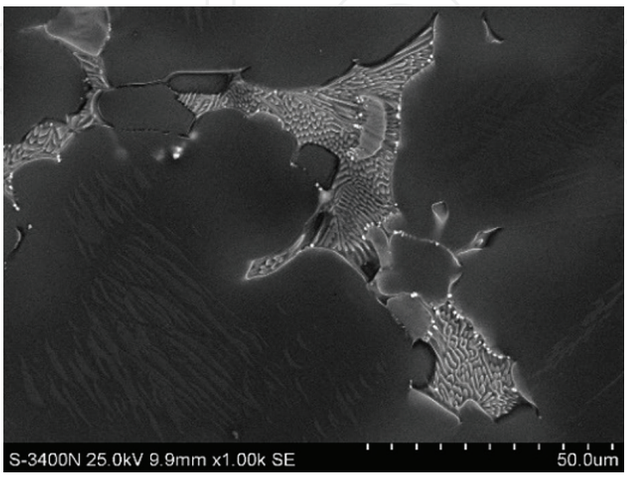

Figure 18. The WE54 alloy microstructure in as-cast condition, SEM.

http://dx.doi.org/10.5772/intechopen.80291

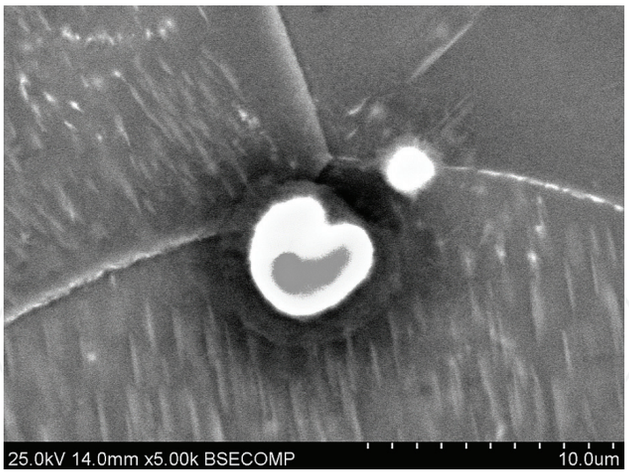

Figure 19. Zirconium-rich core areas in the WE54 alloy.

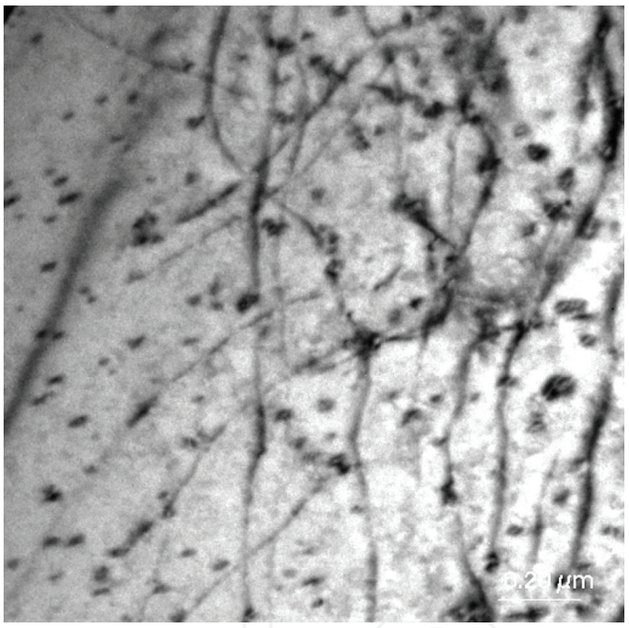

Figure 20. Fine-dispersed precipitates of β″ and β′ phases in the WE54 alloy after aging at 250°C/4 h, TEM.

The high tensile strength of WE54 alloy is related to dispersive precipitations in the microstructure. After 4 hours of aging at 250°C two types of metastable phases, coherent or semi-coherent with the matrix were observed. The first type of precipitates is, coherent with the matrix, β″ phase (**Figure 20**), characterized by type DO_{19} structure [14]. The second phase is, semi-coherent with the matrix β′ phase, characterized by an orthorhombic, space-centered structure [15]. Extension of the aging time up to 16 hours (T6 treatment) causes the disappearance of β″ phase. The β′ phase grows and changes its shape from spherical to lamellar one (**Figure 21**). Extension of the aging time up to 48 h causes the growth and the change of shape of the β′ phase precipitates from spheroidal into lamellar (**Figure 22**) and the beginnings of the phase transformation $\beta' \rightarrow \beta_1$. The resulting new phase, identified as β_1 phase, nucleates heterogeneously on the β′ phase precipitates. The β_1 phase is characterized by a

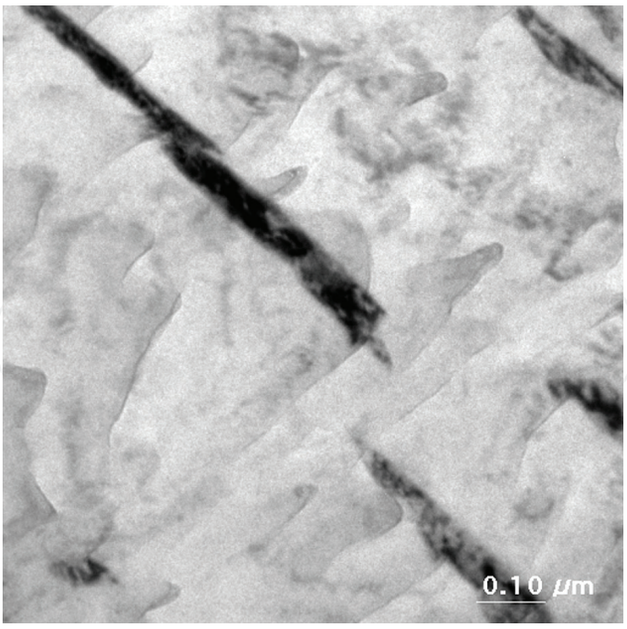

Figure 21. β′ phase precipitates in the WE54 alloy after aging at 250°C/16 h, TEM.

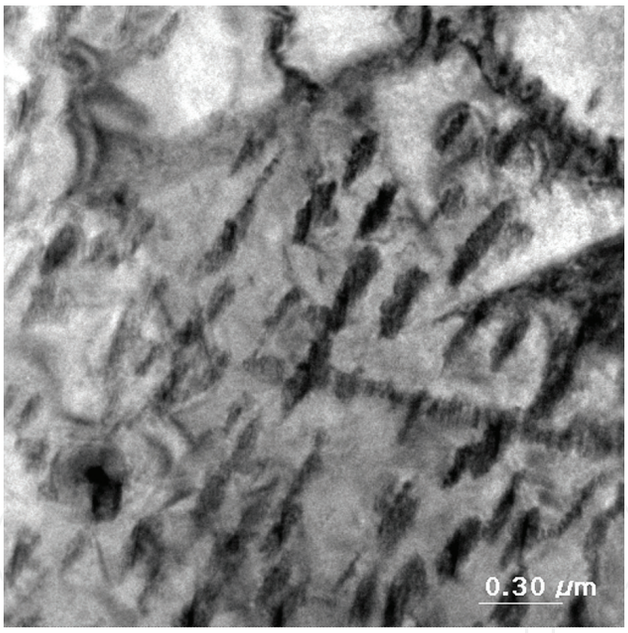

Figure 22. β′ phase precipitates in the WE54 alloy after aging at 250°C/48 h, TEM.

face-centered cubic structure [9]. Further aging (96 h) increases the amount of β_1 phase and causes the emergence of equilibrium β phase (**Figure 23**). Precipitation processes end with the emergence of the equilibrium β phase. It is formed during aging for a long time at 250°C and above (**Figure 24**).

The evolution of hardness and tensile strength as a function of aging time for isothermal aging at 200 and 250°C is shown in **Figure 25**. In practice, for this alloy, aging at 250°C for 16 h is applied (T6 treatment), allowing to obtain maximum tensile strength, which is related to the presence of β″ and β′ phases precipitates in the structure.

http://dx.doi.org/10.5772/intechopen.80291

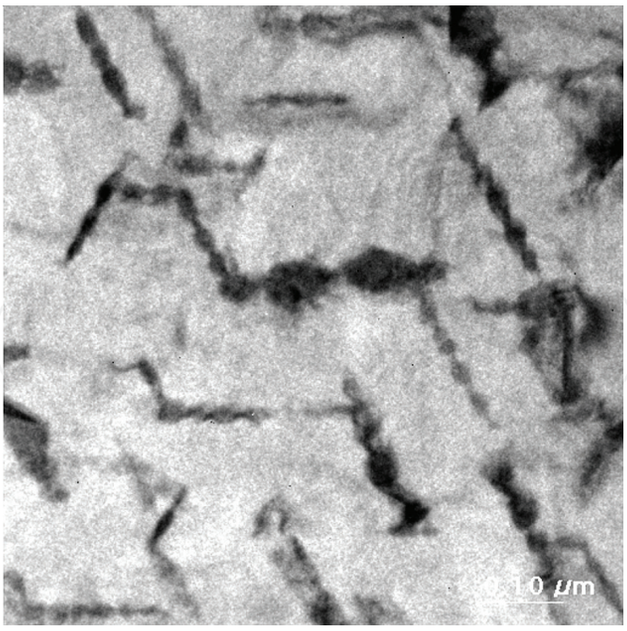

Figure 23. β′ and β1 phases in the WE54 alloy after aging at 250°C/96 h, TEM.

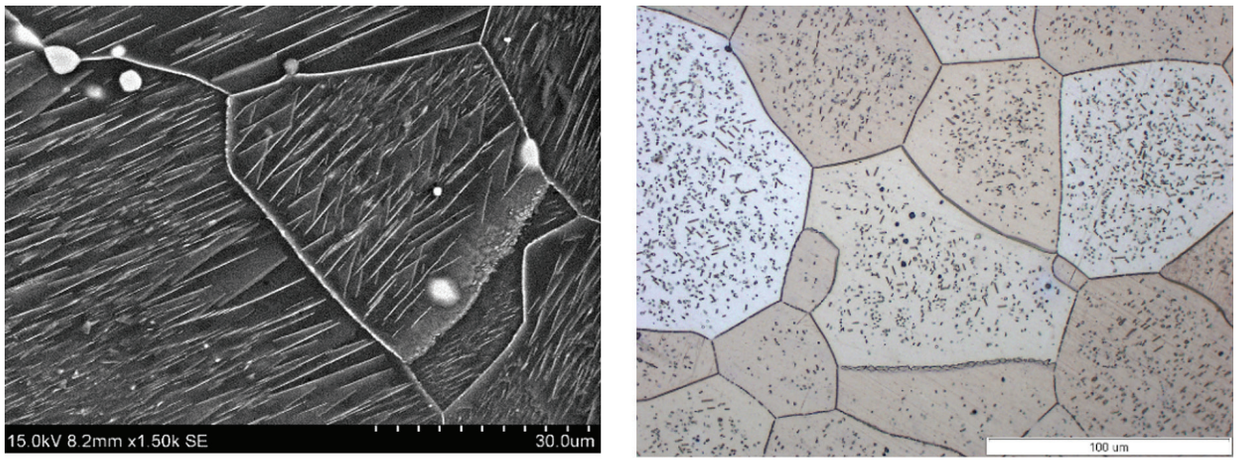

Figure 24. Equilibrium β phase in the WE54 alloy after aging at 300°C/96 h—SEM (a) and 420°C/22 h—LM (b).

The Mg-Y-Zr (WE43 and WE54) alloys are widely used in aircraft and automotive industries. Due to the presence of yttrium, the Mg-Y-Zr alloy belongs to the most expensive of magnesium alloys. This is the main reason for searching other alloys that will fulfill the performance requirements at lower manufacturing costs. One of them is EV31A (Elektron 21) alloy.

6.2. EV31A (Elektron 21) alloy

The EV31A alloy is characterized by the α-Mg solid solution structure with eutectic α-Mg + Mg_3(Nd, Gd) on the grain boundaries and regularly shaped precipitates of a Mg_3Gd phase (**Figure 26**). The Mg_3(Nd, Gd) phase is a modification of Mg_3Nd phase with neodymium substituted by gadolinium without destroying the crystal structure, due to the reasonably small difference in the atomic radii between gadolinium r_{Gd} = 0.1802 nm and neodymium r_{Nd} = 0.1821 nm. Phases occurring in the EV31A alloy take the forms $(Mg, Zn)_3$(Nd, Gd) and $Mg(Gd, Nd)_3$.

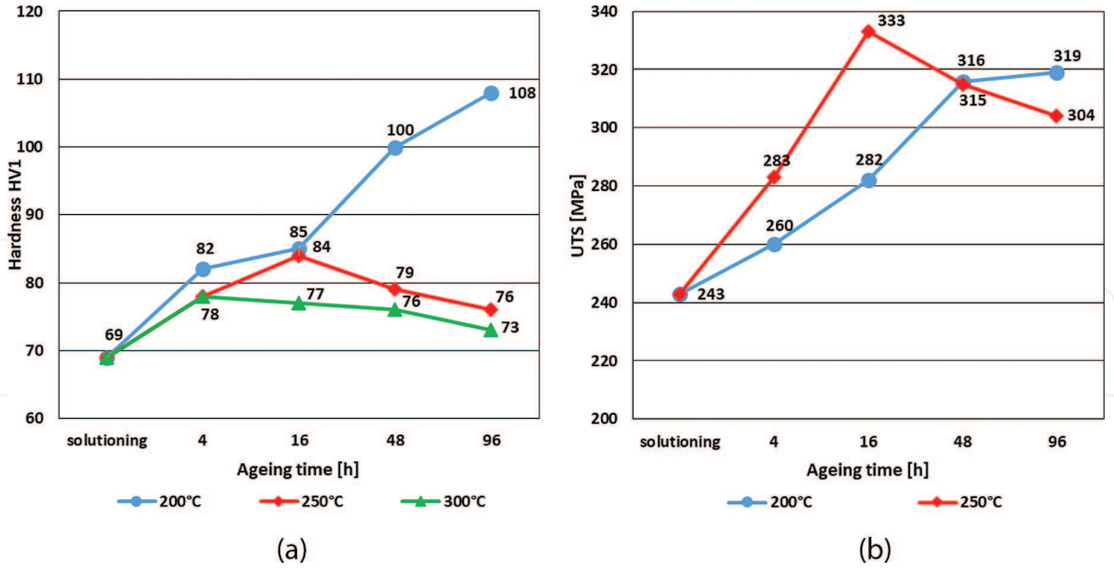

Figure 25. The influence of temperature and annealing time on the hardness (a) and tensile strength (b) of the WE54 alloy.

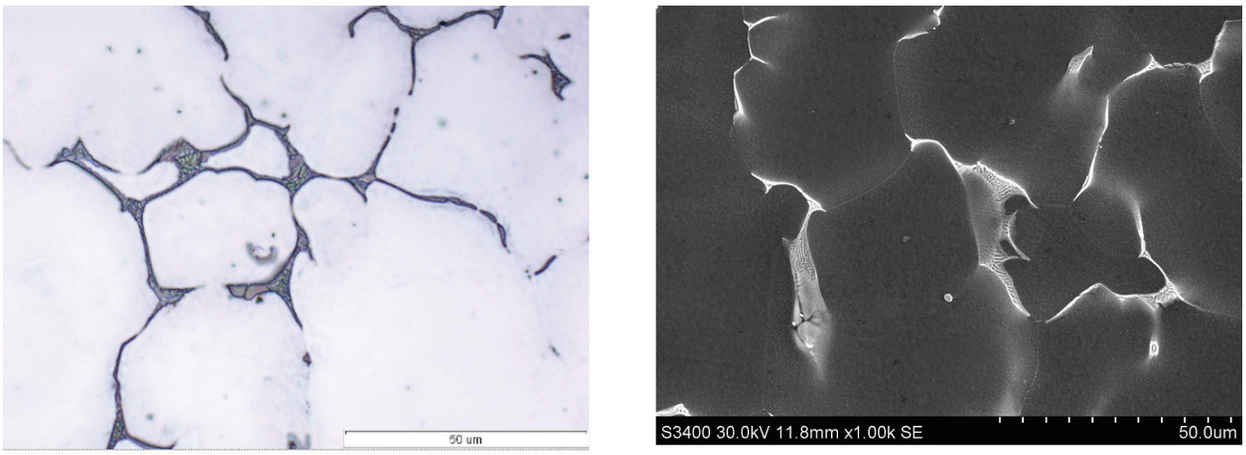

(a) (b)

Figure 26. The EV31A alloy microstructure in as-cast condition, LM (a) and SEM (b).

Similarly, as in the WE54 alloy, high tensile strength is connected with dispersive precipitates produced during aging. In the first stage of the aging process (200°C/4 h and 16 h), the product of the α-Mg decomposition is fully coherent and semi-coherent with the matrix precipitates of β″ and β′ phases, respectively (**Figure 27**).

The β″ phase is characterized by the lattice type DO19 (a = 0.64 nm, c = 0.52 nm), while β′ has a face-centered cubic structure (a = 0.72 nm) [16]. The second stage (200°C/48H) is the formation of a stable equilibrium β(Mg_3Nd) phase. The β phase is non-coherent with the α-Mg matrix. The β phase precipitation process is similar to β_1 phase precipitation in the WE54 alloy. In the immediate vicinity of the β′ phase (**Figure 28**), lamellar precipitates of the equilibrium β phase

http://dx.doi.org/10.5772/intechopen.80291

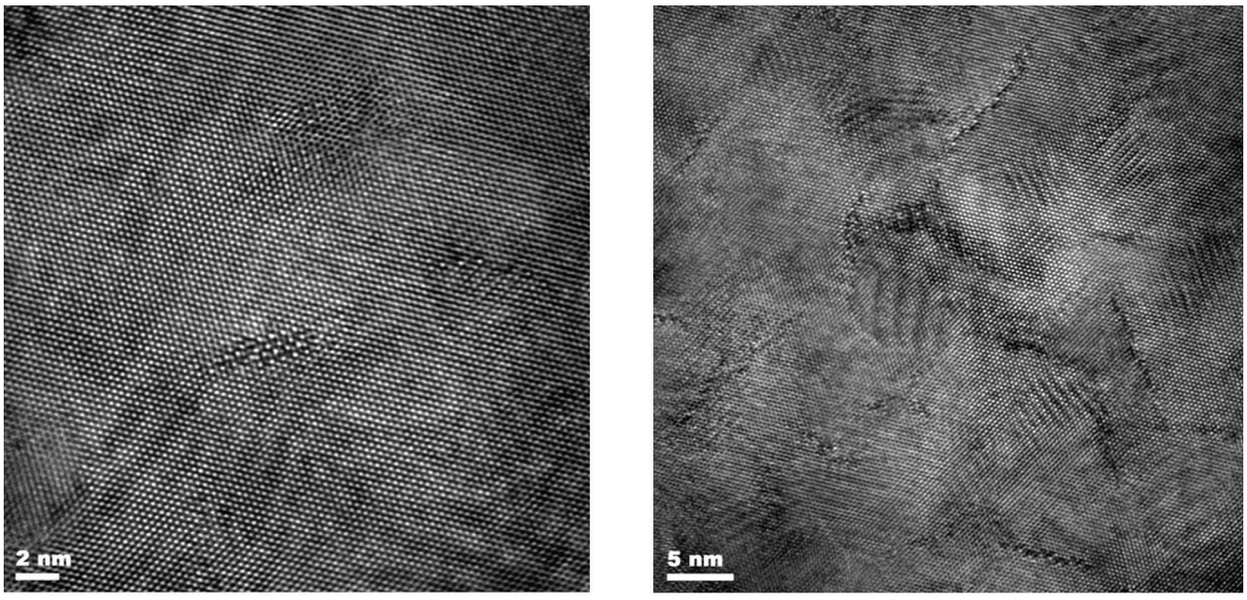

Figure 27. β″ phase precipitates coherent with matrix and separate β′ phase precipitates in EV31A alloy after aging at 200°C/4 h (a) and 200°C/14 h (b), HRTEM image.

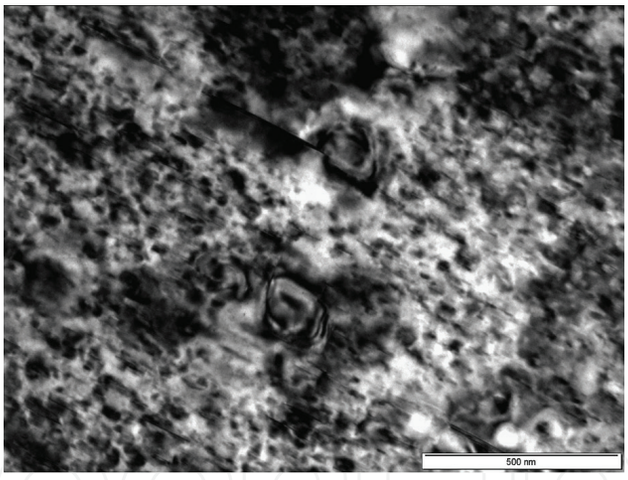

Figure 28. β′ and β phases in the EV31A alloy after aging at 200°C/48 h, TEM.

arise. This indicates that the resulting new phase nucleates heterogeneously at the β′ phase precipitates. After 96 h of aging, the volume fraction of equilibrium β phase increases. The β phase is incoherent with the matrix and identified as an Mg_3Nd phase with face-centered cubic structure (a = 0.7410 nm). On the other hand, aging of this alloy at 300°C leads to the appearance in the structure, next to the lamellar β phase precipitates, of $Mg_{41}Nd_5$ phase precipitates at the solid solution grain boundaries (**Figure 29**).

In the EV31A alloy, after long-term aging at a temperature 350°C/500–5000 h/air, there are no precipitates of equilibrium β phase (**Figure 30**).

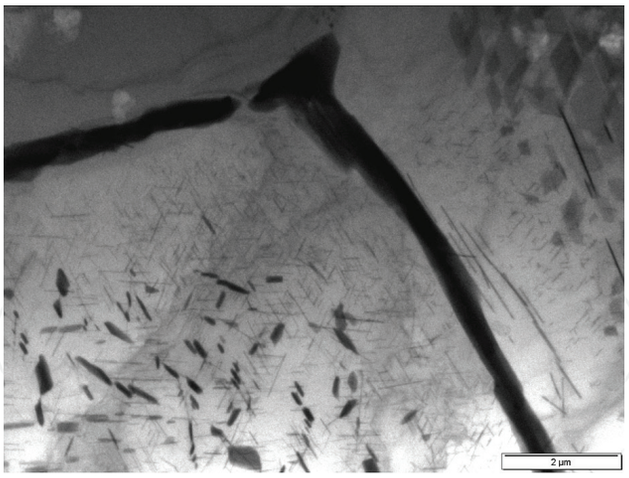

Figure 29. β and Mg41Nd5 phases in the EV31A alloy after aging at 250°C/48 h, TEM.

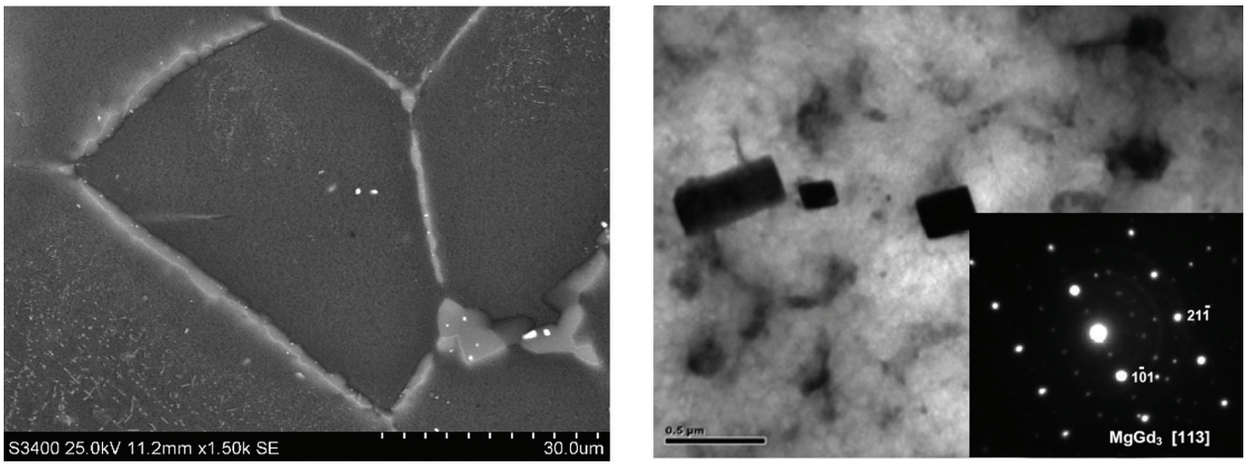

(a) (b)

Figure 30. The microstructure of EV31A alloy after aging at 350°C/1000 h: (a) $Mg_{41}Nd_5$ phase precipitates network at α-Mg solid solution grain boundaries, SEM; (b) TEM image and electron diffraction pattern of MgGd3 phase.

$Mg_{41}Nd_5$ phase creates a characteristic network at the grain boundaries of the α-Mg solid solution. In its vicinity, there are regular $Mg(Nd, Gd)_3$ phase precipitates.

Generally, the investigated alloy showed that the decomposition of α-Mg supersaturated solid solution with increasing aging time is as follows (Eq.(1)):

$$\alpha - \mathrm{Mg} \rightarrow \beta'' \rightarrow \beta' \rightarrow \beta(\mathrm{Mg_3RE}) \rightarrow \mathrm{Mg_{41}Nd_5}. \quad (1)$$

The evolution of hardness and tensile strength as a function of aging time for isothermal aging at 200, 250, and 300°C is shown in **Figure 31**. Alloy showed a remarkable hardening at 200°C temperature, and the peak hardness and good tensile strength can achieve after aging 200°C/16 h due to the precipitation of β″ and β′ phases. The peak hardness was shortened with an increase of the aging temperature. There was not any peak hardness in case of an alloy aged at 300°C. The hardness of EV31A alloy decreases to 45 HV after 500 h of annealing due to precipitation of β and $Mg_{41}Nd_5$ phases.

http://dx.doi.org/10.5772/intechopen.80291

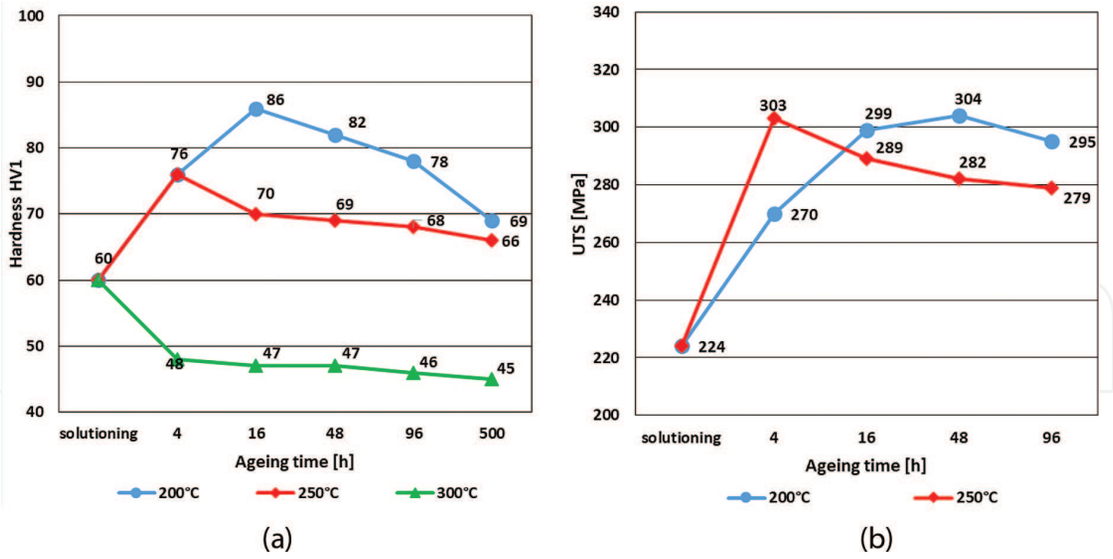

Figure 31. The influence of temperature and annealing time on the hardness (a) and tensile strength (b) of the EV31A alloy.

In practice, for this alloy, aging at 200°C for 16 h is applied (T6 treatment), allowing to obtain maximum tensile strength, which is related to the presence of β″ and β′ phases precipitates in the structure.

7. Conclusions

Results of the research can help in creating conclusions of experience feature, as follows:

1. The AM50 and AZ91 alloys are characterized by the structure of α-Mg solid solution with discontinuous and continuous precipitates of $Mg_{17}Al_{12}$ phase at grain boundaries. The mechanism of precipitation, as well as the volume fraction, morphology, and distribution of $Mg_{17}Al_{12}$ phase, is dependent on temperature and aging time. The $Mg_{17}Al_{12}$ phase undergoes decomposition and coagulation at the temperature above 180°C and higher. The precipitation and degradation processes of this phase in sand-cast result in an increase the hardness of the alloys alongside with lengthening the annealing time. However, in die casts, the coagulation of $Mg_{17}Al_{12}$ phase reduces the hardness of the alloys. The presence of $Mg_{17}Al_{12}$ phase in the structure limits the use of this alloy to a temperature no higher than 120°C.

2. Addition of REs to Mg-Al alloy causes the following phases to form: $Al_{11}RE_3$, Al_2RE, $Al_{2.12}RE_{0.88}$, and $Al_{10}RE_2Mn_7$ in the matrix of the α-Mg solid solution. The microstructure of AE44 alloy during long-term annealing proceeds via two steps. The first step occurs at ~180°C and is characterized by precipitation of the $Mg_{17}Al_{12}$ phase (mainly for sand casting) in areas of higher aluminum volume and by the appearance of changing $Al_{2.12}RE_{0.88} \rightarrow Al_2RE$ (for die casting). The process of precipitation of the $Mg_{17}Al_{12}$ phase is only the result of continuous precipitation in areas of higher aluminum volume. The $Al_{11}RE_3$ phase is stable up to 250°C. The second step stage takes place at a temperature equal to or higher than 250°C and is characterized by significant degradation of the structure, which is manifested by fragmentation and spheroidization of the $Al_{11}RE_3$ phase. The degradation of $Al_{11}RE_3$ phase caused a significant decrease in hardness and tensile strength of die casting AE44.

3. The AJ62 alloy is characterized by the structure of the α-Mg solid solution with precipitates of intermetallic phases of type: (Al, Mg)$_4$Sr, Al$_3$Mg$_{13}$Sr, and Mn$_5$Al$_8$. The (Al, Mg)$_4$Sr phase and the solid solution form eutectic of α-Mg + (Al, Mg)$_4$Sr. Long-term annealing of this alloy at temperatures 180 and 250°C causes decomposition of Al$_3$Mg$_{13}$Sr phase according to the reaction Al$_3$Mg$_{13}$Sr → (Al, Mg)$_4$Sr + α-Mg, while at the temperature of 350°C, it leads to fragmentation and coagulation of (Al, Mg)$_4$Sr phase. Observed microstructure changes cause a decrease of mechanical properties of the alloy.
4. The WE54 alloy is characterized by the structure of the α-Mg solid solution with eutectic α-Mg + β(Mg$_{14}$Y$_2$Nd). Moreover, the occurrence of MgY, Mg$_2$Y, and Mg$_{24}$Y$_5$ phases has been provided. During aging, the supersaturated magnesium solid solution decomposes in the following sequence α-Mg → β″ → β′ → β$_1$ → β. The WE54 alloy is widely used in aircraft and automotive industries for components utilized up to a temperature of ~250°C. However, due to its price, there is a search for other alloys, which can fulfill the performance requirements at lower manufacturing costs. One of such alloys is the EV31A alloy.
5. The EV31A alloy is characterized by the α-Mg solid solution structure with the eutectic α-Mg + (Mg, Zn)$_3$(Nd, Gd) at the grain boundaries of the α-Mg solid solution and regularly shaped, MgGd$_3$ phase precipitates. The precipitation process during aging runs in accordance with the sequence: α-Mg → β″ → β′ → β(Mg$_3$Nd) → Mg$_{41}$Nd$_5$. The obtained results indicate that the EV31A alloy can be utilized at temperatures up to ~200°C and can be a substitute for the previously used WE54 alloy.

Acknowledgements

The present work was financed from the research project no. 11/990/BK_18/0057.

Author details

Andrzej Kiełbus

Address all correspondence to: andrzej.kielbus@polsl.pl

Silesian University of Technology, Katowice, Poland

References

[1] Friedrich H, Mordike B. Magnesium Technology. Berlin Heidelberg: Springer-Verlag; 2006. 677 p. DOI: 10.1007/3-540-30812-1

[2] Mordike B, Eberr T. Magnesium: Properties-applications-potentials. Materials Science and Engineering: A. 2001;**302**:37-45. DOI: 10.1016/S0921-5093(00)01351-4

[3] Pettersen G, Westengen H, Høier R, Lohne O. Microstructure of a pressure die-cast magnesium-4wt.% aluminum alloy modified with rare earth additions. Materials Science Engineering: A. 1996;**207**:115-120. DOI: 10.1016/0921-5093(95)10035-0

[4] Bakke P, Westengen H. The role of rare earth elements in structure and property control of magnesium die casting alloys. In: Mathaudhu S, Luo A, Neelameggham N, Nyberg E, Sillekens W, editors. Essential Readings in Magnesium Technology. Cham, Springer International Publishers; 2005. pp. 313-318. DOI: 10.1007/978-3-319-48099-2_50

[5] Powell BR, Rezhets V, Balogh MP, Waldo RA. Microstructure and creep behavior in AE42 magnesium die-casting alloy. The Journal of The Minerals, Metals & Materials Society. 2002;**54**(8):34-38. DOI: 10.1007/BF02711864

[6] Yang M, Pan F, Zhang J. An analysis of the development and applications of current and new Mg-Al based elevated temperature magnesium alloys. Materials Science Forum. 2005;**488-489**:923-926. DOI: 10.4028/www.scientific.net/MSF.488-489.923

[7] Parvez MA, Medraj M, Essadiqi F, Muntasar A, Denes G. Experimental study of the ternary magnesium—Aluminum–strontium system. Journal of Alloys and Compounds. 2005;**402**:170-185. DOI: 10.1016/j.jallcom.2005.04.173

[8] Czerwinski F, Zielinska-Lipiec A. The microstructure evolution during semisolid molding of a creep-resistant Mg-5Al-2Sr alloy. Acta Materialia. 2005;**53**(12):3433-3444. DOI: 10.1016/j.actamat.2005.03.048

[9] Nie JF, Muddle BC. Precipitation in magnesium alloy WE54 during isothermal aging at 250°C. Scripta Materialia. 1999;**40**(10):1089-1094. DOI: 10.1016/S1359-6462(99)00084-6

[10] Rokhlin LL, Dobatkina TV, Tarytina IE, Timofeev VN, Balakhchi EE. Peculiarities of the phase relations in Mg-rich alloys of the Mg-Nd-Y system. Journal of Alloys and Compounds. 2004;**367**:17-19. DOI: 10.1016/j.jallcom.2003.08.004

[11] Kielbus A. Microstructure and properties of elektron 21 magnesium alloy. In: Czerwinski F, editor. Magnesium Alloys. London: IntechOpen; 2011. pp. 281-296. DOI: 10.5772/13220

[12] Lyon P, Syed I, Wilks T. The influence of alloying elements and heat treatment upon properties of Elektron 21 (EV31A) alloy. In: Proceedings of Magnesium Technology—Symposium; 13-17 February 2005; USA. San Francisco: TMS; 2005. pp. 303-308

[13] Kielbus A. Microstructure and properties of sand casting magnesium alloys for elevated temperature applications. Solid State Phenomena. 2011;**176**:63-74. DOI: 10.4028/www.scientific.net/SSP.176.63

[14] Antion C, Donnadieu P, Perrard F, Deschamps A, Tassin C, Pisch A. Hardening precipitation in a Mg–4Y–3RE alloy. Acta Materialia. 2003;**51**:5335-5348. DOI: 10.1016/S1359-6454(03)00391-4

[15] Nie JF, Xiao XL, Luo CP, Muddle BC. Characterisation of precipitate phases in magnesium alloys using electron microdiffraction. Micron. 2001;**32**:857-863. DOI: 10.1016/S0968-4328(00)00094-9

[16] He SM, Zeng XQ, Peng LM, Gao X, Nie JF, Ding WJ. Precipitation in a Mg–10Gd–3Y–0.4Zr (wt.%) alloy during isothermal ageing at 250°C. Journal of Alloys and Compounds. 2006;**421**:309-313. DOI: 10.1016/j.jallcom.2005.11.046

IntechOpen